EurJIC
European Journal of Inorganic Chemistry

Full Paper
doi.org/10.1002/ejic.202000413

Intermetallic Phases

From Zintl to Wade: Ba_3LiGa_5 – A Structure Pattern with Pyramidal Cluster Chains $–[Ga_5]_n–$

Matthias Kotsch,*[a] Yurii Prots,[a] Alim Ormeci,[a] Matej Bobnar,[a,b] Frank R. Wagner,[a] Anatoliy Senyshyn,[c] and Yuri Grin*[a]

Abstract: Investigation of the correlation between the crystal structure, electronegativity difference and valence electron concentration in intermetallic gallides lead to the discovery of the new compound Ba_3LiGa_5 (space group *Immm*, a = 6.2720(2) Å, b = 6.5872(2) Å, c = 12.6878(8) Å). A combination of quantum chemical bonding analysis with NMR study revealed the gallium substructure to be formed of chains built of the interconnected pyramidal $[Ga_5]$ clusters. Analysis of chemical bonding by means of the electron localizability approach confirmed the presence *nido*-$[Ga_5]$ Wade clusters. Lithium species are not only required for the purpose of charge compensation, but also – analogous to a transition metal – occupies partially the same crystallographic position as gallium.

Introduction

Intermetallic compounds containing discrete gallium cluster units are mainly found in systems *M*–Ga, where *M* is an alkali, alkaline-earth metal, europium or uranium.[1] In the chemically related compounds of boron, the homoatomic connectivity of the boron atoms is often described as related to its content. With the decreasing boron concentration, the boron arrangements vary from isolated cluster units through 3D frameworks, 2D networks, linear chains toward isolated atoms.[2–4] In the case of gallium, such tendency is not recognizable.[5] Moreover, systematic analysis of the compounds of gallium with yttrium revealed charge transfer and the valence electron concentration as main characteristics of atomic interactions.[6] Applying such approach on the gallium connectivity in MGa_n compounds, allows to distinguish the stability fields for the different gallium arrangements in terms of the electronegativity difference between the constituent components (ΔEN) and number of valence electrons available per gallium atom (VEC_{Ga}, Figure 1). Such representation allows, e.g., the understanding of structural difference between Eu_3Ga_5[15] and $Eu_3Li_{5+x}Ga_{5-x}$.[5] Here, the introduction of lithium increases the VEC_{Ga} and reduces the ΔEN.

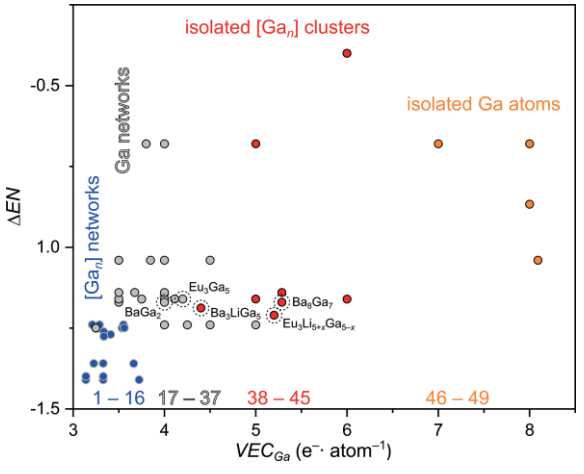

Figure 1. Gallium arrangements in MGa_n phases, where *M* is an alkali, alkaline-earth metal, europium or uranium, in dependence on the VEC_{Ga} and electronegativity difference of the components ΔEN: interlinked $[Ga_n]$ networks (blue), Ga networks (grey), isolated $[Ga_n]$ clusters (red) and isolated Ga atoms (orange): 1 = $CsGa_7$, 2 = $RbGa_7$, 3 = Li_3Ga_{14}, 4 = K_3Ga_{13}, 5 = $LiGa_{3.42}$, 6 = $RbGa_3$, 7 = KGa_3, 8 = $CsGa_3$, 9 = $Rb_{0.6}Na_{6.25}Ga_{20.32}$, 10 = $K_4Na_{13}Ga_{50}$, 11 = $K_3Li_9Ga_{29}$, 12 = Na_7Ga_{13}, 13 = Li_5Ga_9, 14 = $Na_{22}Ga_{39}$, 15 = K_2Ga_3, 16 = Cs_8Ga_{11}, 17 = $NaGa_4$, 18 = $BaGa_4$, 19 = $EuGa_4$, 20 = $SrGa_4$, 21 = $CaGa_4$, 22 = $Sr_{2.85}Ga_{8.45}$, 23 = Eu_3Ga_8, 24 = Mg_2Ga_5, 25 = $CaGa_{2.36}$, 26 = $EuGa_2$, 27 = $SrGa_2$, 28= $BaGa_2$, 29 = $CaGa_2$, 30 = LiGa, 31 = $MgGa_2$, 32 = Eu_5Ga_9, 33 = Eu_3Ga_5, 34 = Li_5Ga_4, 35 = Ca_3Ga_4, 36 = Li_3Ga_2, 37 = Li_2Ga, 38 = Ba_3LiGa_5, 39 = EuGa, 40 = MgGa, 41 = $Eu_3Li_{5+x}Ga_{5-x}$, 42 = Sr_8Ga_7, 43 = Ba_8Ga_7, 44 = Eu_3Ga_2, 45 = U_3Ga_5, 46 = Mg_2Ga, 47 = $LiMg_2Ga$, 48 = Mg_5Ga_2, 49 = $Ca_{28}Ga_{11}$. Compounds sorted in ascending order with respect to VEC_{Ga} and ΔEN. Crystallographic information is taken from refs.[5, 7–13]; electronegativity values according to Sanderson;[14] $\Delta EN = \Sigma(n_{cation}\cdot EN_{cation})/(\Sigma n_{cation}) - EN_{Ga}$; $VEC_{Ga} = \Sigma(n_{valence\ electrons})/n_{Ga}$.

[a] *M. Kotsch, Dr. Yu. Prots, Dr. A. Ormeci, Dr. M. Bobnar, Dr. F. R. Wagner, Prof. Yu. Grin*
Chemische Metallkunde, Max-Planck-Institut für Chemische Physik fester Stoffe,
Nöthnitzer Straße 40, 01187 Dresden, Germany
E-mail: kotsch@cpfs.mpg.de
grin@cpfs.mpg.de
[b] *Dr. M. Bobnar*
Jožef Stefan Institute,
Jamova 39, SI1000 Ljubljana, Slovenia
[c] *Dr. A. Senyshyn*
Forschungsneutronenquelle Heinz Maier-Leibnitz (FRM II),
Technische Universität München,
Lichtenbergstrasse 1, 85747 Garching b. München, Germany
Supporting information and ORCID(s) from the author(s) for this article are available on the WWW under https://doi.org/10.1002/ejic.202000413.

Full Paper
doi.org/10.1002/ejic.202000413

As a consequence, the three-dimensional Ga framework in Eu_3Ga_5 is transformed into isolated bell-like clusters [Ga_5] in $Eu_3Li_{5+x}Ga_{5-x}$. Transferring such trend to the chemically analogous system Ba–Ga, one finds already its confirmation in the transformation of two–dimensional honeycomb nets of gallium in $BaGa_2$ (structure type AlB_2)[16] into the cluster units [Ga_4] and [Ga_3] in Ba_8Ga_7[9] (Figure 1). In analogy to the europium system above, one would expect a similar transformation of this two–dimensional Ga network into isolated cluster units in a ternary Ba–Li–Ga compound. During the experimental attempts to prove the trend above, the compound Ba_3LiGa_5 has been isolated and investigated. Preliminary results of this work were presented at a conference.[17]

Results and Discussion

Structure Determination

The orthorhombic unit cell was established from the single-crystal investigation, and the lattice parameters were refined from the X-ray powder diffraction data: a = 6.2720(2) Å, b = 6.5872(2) Å and c = 12.6878(8) Å. The evaluation of the single-crystal diffraction patterns for systematic extinctions resulted in the possible space groups $I222$, $I2_12_12_1$, $Imm2$ and $Immm$. During the following structure solution and refinement, $Immm$ was found as the correct one. The initial solution of the structure was performed by using the direct methods, yielding a first model with the composition Ba_3Ga_6. An analysis of the isotropic displacement parameters at this stage revealed an anomaly of the atomic displacement parameters at the Ga1 position (U_{iso}(Ga1) >> U_{iso}(Ga2) ≈ U_{iso}(Ga3)). Refinement of the occupancy of this position as a Ga/Li mixture (denoted as X1 site) resulted in the composition $Ga_{0.499(4)}Li_{0.501}$. A second anomaly was found for Ba2 upon refinement of the anisotropic displacement parameters: U_{33} >> U_{11} ≈ U_{22}. To take this into account, Ba2 was described by a split position. The total composition after refinement is $Ba_3Li_{1.002}Ga_{4.998}$. It was confirmed by the results of the chemical analysis and neutron powder diffraction (**Figure S7**). Attempts to resolve the positions of Li and Ga at the X1 site were not successful neither with the single-crystal X-ray diffraction nor with the neutron powder diffraction data. The crystallographic data, final atomic coordinates, displacement parameters are listed in Table 1 and Table 2 and interatomic distances in **Table S1.**

Deposition Number 2001150 contains the supplementary crystallographic data for this paper. These data are provided free of charge by the joint Cambridge Crystallographic Data Centre and Fachinformationszentrum Karlsruhe Access Structures service www.ccdc.cam.ac.uk/structures.

Structure Description

The central recurring motif in Ba_3LiGa_5, is a tetragonal pyramid [Ga_5] formed by the gallium atoms. This cluster is capped over the quadrangular face by a lithium atom, forming the heteronuclear, octahedral assembly [$LiGa_5$] (Figure 2 **top**). The orientation of the [Ga_5] pyramids is random, resulting in the equal occupation of Li and Ga at the 4*g* position above and below the quadrangular plane. Within each pyramid, three different Ga–Ga distances are found, due to a slight skewing of the base in the [001] direction from 2.667(1) Å for the base itself to 2.610(1) Å and 2.712(1) Å for the contacts between the corners and the apex (Figure 2 **middle**). The pyramids are interconnected into chains via Ga–Ga contacts of 2.647(1) Å at opposing corners of the base along [100]. Each chain has two adjacent chains within the (101) plane, with a distance of d(X1–X1) = 2.830(2) Å. This can formally be described as 2D slabs of interlinked [$LiGa_5$] octahedra (Figure 2 **top**) stacked along [001] and shifted by (1/2 1/2 0) with respect to each other and a distance of 5.156(4) Å.

Table 1. Crystallographic data for Ba_3LiGa_5.

Composition	Ba_3LiGa_5
Crystal system	orthorhombic
Space group	*Immm* (no. 71)
Formula units per cell, Z	2
Lattice parameters[a]	
a / Å	6.2720(2)
b / Å	6.5872(2)
c / Å	12.6878(8)
V / Å ^{3}	524.19(4)
Calc. density / g cm^{-3}	4.86
Crystal shape	irregular
Crystal size / mm	0.045 × 0.085 × 0.090
Diffraction system	Rigaku AFC7
Detector	Saturn 724+ CCD
Wavelength (radiation) / Å	0.71073 (MoK_α)
Scan; N(images); 2Θ step / deg	ϕ, 1200, 0.6
Maximal 2Θ / deg	85.9
Ranges *hkl*	$-11 \le h \le 4$
	$-10 \le k \le 12$
	$-24 \le l \le 20$
Absorption correction	multi-scan
μ /mm^{-1}	23.62
F(000)	651.8
N(*hkl*) measured	5108
N(*hkl*) unique	1111
R_{Int}	0.046
N(*hkl*) observed	959
Observation criteria	F(*hkl*) > 4 σ(F)
Refined parameters	20
Goof	1.03
$R(F)$[F(*hkl*) > 4 σ(F)]	0.032
Rw	0.035
Residual peaks / e Å $^{-3}$	1.52, –1.27

[a] Obtained from the positions of 105 reflections extracted from powder X-ray data (Huber G670 Imaging Plate Guinier camera, Cu$K_{\alpha1}$ radiation: λ = 1.54056 Å, 14.0 < 2Θ < 98.1).

Table 2. Atomic coordinates and equivalent displacement parameters (in Å^2) in the crystal structure of Ba_3LiGa_5 (space group *Immm*).

Atom	Wyckoff site	x	y	z	U_{eq}
Ba1	4*j*	1/2	0	0.24834(4)	0.0167(1)
Ba2[a]	4*i*	0	0	0.4894(2)	0.0200(5)
X1[b]	4*g*	0	0.2852(3)	0	0.0154(4)
Ga2	4*i*	0	0	0.15419(8)	0.0166(2)
Ga3	4*e*	0.2890(2)	0	0	0.0195(2)

[a] Ba2 occupancy = 0.5. [b] X1 occupancy by Ga and Li is refined to 0.499(4):0.501.

Full Paper
doi.org/10.1002/ejic.202000413

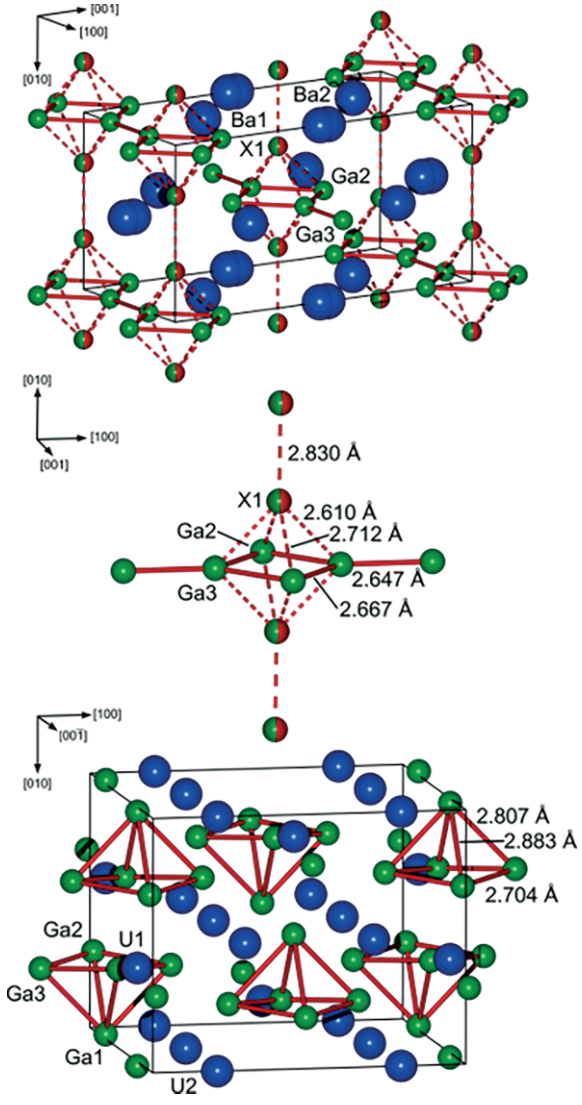

Figure 2. Crystal structure of Ba_3LiGa_5: (top) unit cell with Ga–Li arrangements; (middle) interatomic distances in the Ga–Li framework; (bottom) isolated pyramidal Ga arrangements in U_3Ga_5.

The distinct motif of [Ga_5] pyramids has previously been observed in U_3Ga_5 (space group *Cmcm*, Pu_3Pd_5–structure type (Figure 2 **bottom**). In comparison, it can be observed, that the Ga–Ga contacts, which make up the base of the pyramid are slightly shorter in Ba_3LiGa_5 (2.667(1) Å) than in U_3Ga_5 (2.704 Å). Both compounds exhibit a deviation from an ideal pyramid, with U_3Ga_5 having a slightly puckered base and the Ba_3LiGa_5 base being skewed along the [001] direction (∠Ga2–Ga3–Ga2 = 94.4°; ∠Ga3–Ga2–Ga3 = 85.6°). This leads to two different distances for the Ga–Ga contacts between the base and the apex of the pyramid in both compounds (2.610(1) Å/2.712(1) Å in Ba_3LiGa_5; 2.807 Å/2.883 Å in U_3Ga_5). The surrounding cationic arrangement however, varies greatly between the two compounds. While the uranium atoms in U_3Ga_5 merely surrounds the [Ga_5] pyramids in an irregular arrangement, each [$LiGa_5$] octahedron in Ba_3LiGa_5 is enclosed by a slightly distorted cuboctahedron formed by barium with interatomic Ba–Ba distances ranging from 4.381(2) Å to 4.652(2) Å. The Ba–Ga distances vary from 3.3558(4) Å to 3.5522(3) Å. This is in agreement with the reported values in binary phases, e.g., *d*(Ba–Ba) = 4.432 Å and *d*(Ba–Ga) = 3.606 Å in $BaGa_2$.[16]

In order to resolve the mixed occupation and create ordered models suitable for quantum chemical calculations, five structure models (Figure 3) were developed using the group-subgroup approach (**Figure S1**). These are either an alternating orientation of the pyramids, as seen in model **4**, or a common orientation in one direction as displayed in models **1**, **2**, **3** and **5**. Due to the appearance of Li–Li contacts however, the models **3** and **5** were seen as less plausible, which was later confirmed by the quantum chemical calculations. The remaining two models **1** and **2** are almost identical, with the only difference being the parallel or antiparallel orientation of the slabs with respect to each other. The observed mixed occupation of the 4*g* position in the space group *Immm*, can be interpreted as a superposition of these two models.

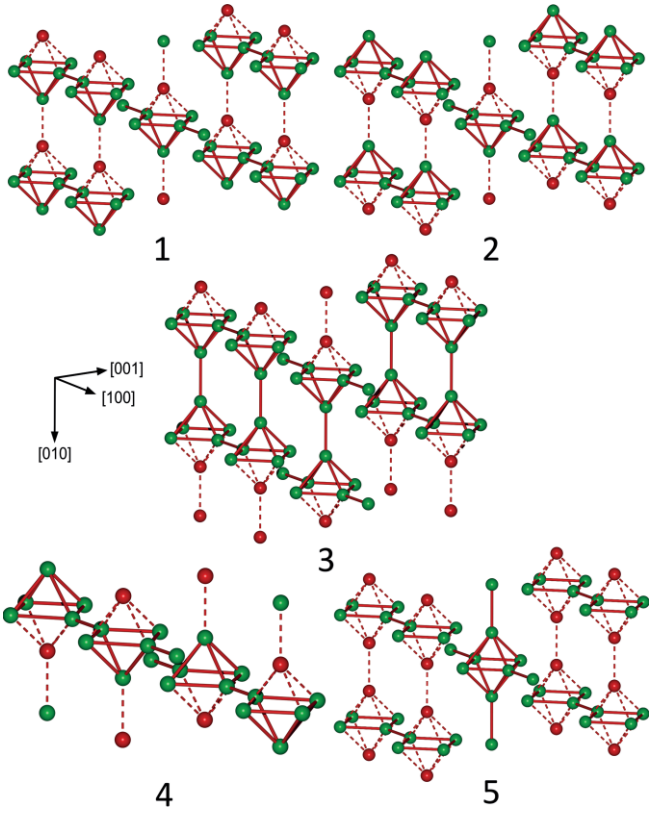

Figure 3. Ordered models of Ba_3LiGa_5: **(1)** space group *Im*2*m*, $a = a_0$, $b = b_0$, $c = c_0$; **(2)** space group *Pmnm*, $a = a_0$, $b = b_0$, $c = c_0$; **(3)** space group *Pmnm*, $a = a_0$, $b = 2b_0$, $c = c_0$; **(4)** space group *Pnam*, $a = 2a_0$, $b = b_0$, $c = c_0$; **(5)** space group *Pmmm*, $a = a_0$, $b = b_0$, $c = c_0$. The coordinate axis directions and lattice parameters a_0, b_0, c_0 of the refined model of Ba_3LiGa_5 are as in the Table 1 and Table 2. Ba atoms are omitted for clarity.

The total energies computed for the considered ordered models of Ba_3LiGa_5 indicate that the models **1** and **2** are essentially degenerate. Therefore, the total energy of model **2** is set to 0 eV. Models **1** and **4** have slightly higher energies of +1.21 and +2.93 meV/f.u., respectively. Close energies of all three models are the reason for non-ordered orientation of the [Ga_5] clusters in the crystal structure. The energies of models **3** and **5** are much higher: +515 and +774 meV/f.u. (non-optimized),

Full Paper
doi.org/10.1002/ejic.202000413

respectively. Moreover, analysis of the electronic structure shows that these models have electronic density of states characteristic for metals (no gap), whereas the lower-energy models have small band gaps (Figure 4); their DOS curves are almost identical. Thus, models **3** and **5** are not considered further. The calculated band gap values are 0.23, 0.23 and 0.29 eV for the models **1**, **2** and **4**, respectively. The narrow states between –9 and –8.5 eV are mostly due to the Ga 4*s* electrons. The three peaks located around –6.5, –5.7 and –4.5 eV are contributed mainly by the 4*s* states of Ga2, Ga3 and Ga1, respectively. Ga 4*p* contributions become dominant above –2.5 eV. Between this value and the top of the valence band (set to 0 eV) Li 2*s* as well as Ba 5*d* contributions are also important. The low energy part of the conduction band is dominated by Ba 5*d* states. The electron energy band dispersions (**Figure S4**) confirm that the models **1**, **2** and **4** of Ba_3LiGa_5 represent indirect gap semiconductors.

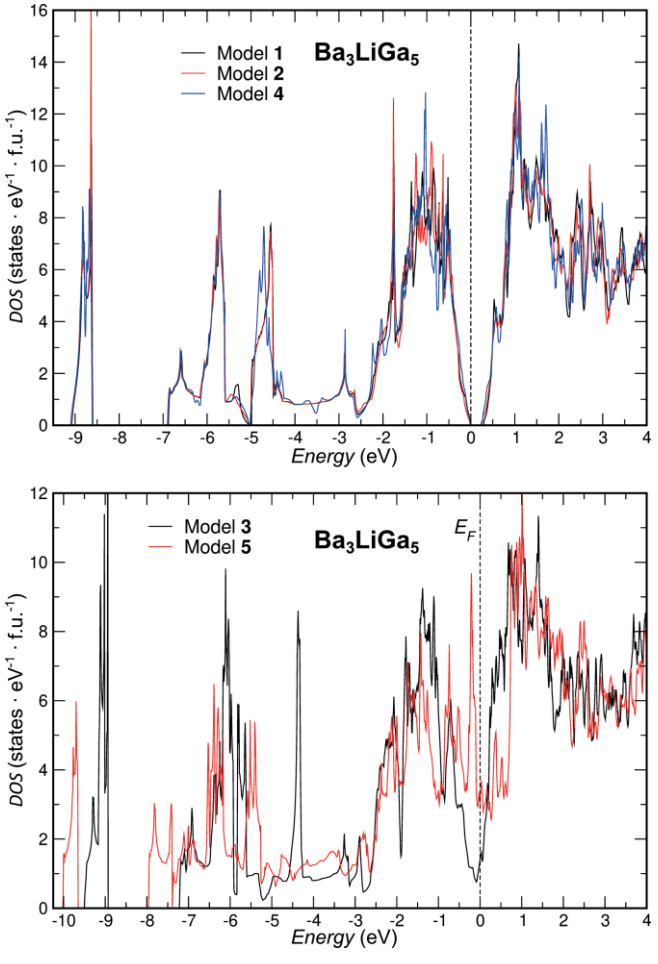

Figure 4. Electronic density of states of Ba_3LiGa_5 for the models **1**, **2**, **4** (upper panel) and **3** and **5** (bottom panel).

NMR Study

For an additional confirmation of the structure, we investigated the local atomic environments in Ba_3LiGa_5 using ^7Li and ^{71}Ga static, magic angle spinning (MAS) NMR on pre-oriented polycrystalline material.[18–20] The static ^7Li spectrum (Figure 5 **top**) consists of a broad central line and a bell–shaped satellite background with some distinct features, whereas the MAS spectrum shows two signals. A large one with the isotropic shift of 1.3 kHz and the relative intensity of 89 %, which belongs to the Li atoms located on the X1 crystallographic position, and a small one with the shift of 0.1 kHz, which most likely originates from the decomposition products resulting from the specimen preparations. The peaks at ±25 kHz are the rotational sidebands (Figure 5). From the ^7Li NMR data, only one local Li configuration (cf. models **1, 2, 4**) is confirmed.

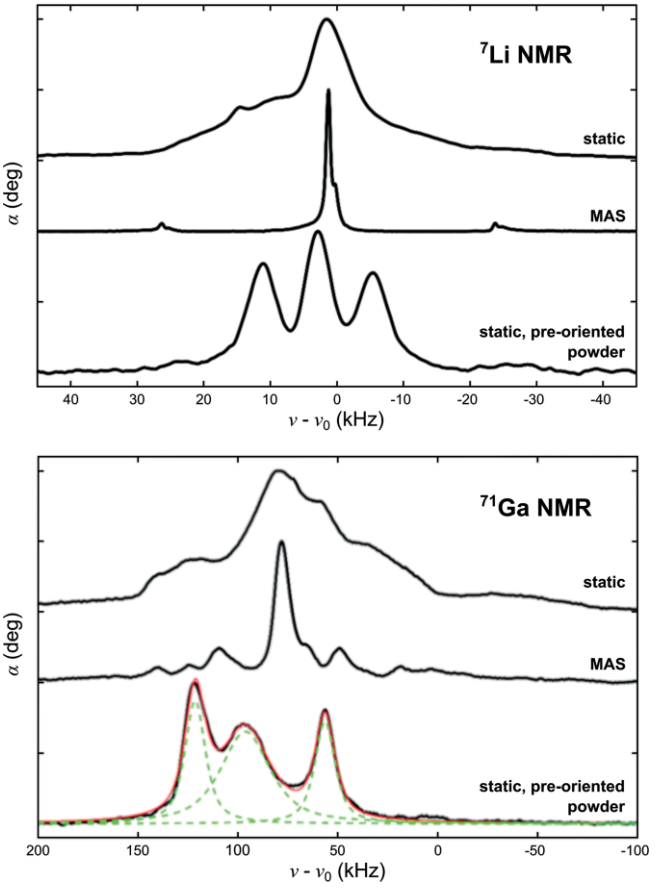

Figure 5. NMR study of Ba_3LiGa_5: ^7Li NMR (upper panel); ^{71}Ga NMR (bottom panel). Each panel shows static spectrum (top); MAS at 25 kHz (middle) and NMR on pre-oriented polycrystalline material (bottom).

The ^{71}Ga NMR is more complex, since there are three crystallographic positions for Ga, one of them – Ga1 – being half-occupied by Li (denoted as X1 in Table 2). The quadrupole coupling constant for ^{71}Ga is also much larger, so that the satellite transitions are not observable close to the Larmor frequency. However, the frequency of the central transition is affected by the quadrupole coupling in the second order showing a broad static spectrum with several characteristic features (Figure 5), which could not be satisfactorily fit by a model with three signals, broadened by the second order quadrupole coupling and chemical anisotropy. The MAS did not improve the resolution. However, the pre-oriented powder clearly shows three distinct ^{71}Ga NMR signals, shifted by 57 kHz, 96 kHz, and 121 kHz and with the area of the fitted peaks in the ratio of 23 %, 49 %, and

Full Paper
doi.org/10.1002/ejic.202000413

28 %, respectively. The peak at 57 kHz may be assigned to the signal from Ga1 due to the lowest intensity. Assuming the polarisation influence of the Ba and Li neighbors, one may speculate that the signal around 95 kHz reflects the Ga3 position, and the signal around 120 kHz originates from Ga2. However, an unambiguous assignment of these two peaks remains an open question.

Chemical Bonding Analysis

The striking feature of the crystal structure of Ba_3LiGa_5 is a two–dimensional slabs of stacked chains consisting of the homoatomic pseudo-tetragonal pyramids [Ga_5]. Considering the shortest interatomic Ga–Ga distances as bonding, the composition and the atomic arrangement of Ba_3LiGa_5 can be understood formally within the Zintl–Klemm concept with the electronic balance $[Ba^{2+}]_3[Li^{1+}]_1[(3b)Ga^{2-}]_2[(4b)Ga^{1-}]_3$.

Interestingly, the description of the structure can be made also using the Wade–Mingos rules.[21,22] According to the latter, the two-connected pyramidal *nido*-cluster $[Ga_5]^{7-}$ requires 14 skeletal electrons for stabilization, 2 electrons for two inter-cluster Ga–Ga bonds and six electrons for three lone pairs on the gallium atoms, which do not participate at homoatomic inter-cluster bonds. In total, the formula unit Ba_3LiGa_5 possesses 22 valence electrons, i.e. also this counting scheme is charge balanced.

Taking into account the slightly smaller electronegativity of Li in comparison with that of Ba (after Sanderson), one may consider Li–Ga interaction as polar covalent, i.e., lithium atoms become part of the octahedral heteroatomic cluster [$LiGa_5$], which requires also 14 skeletal electrons for its stabilization. Contrary to $[Ga_5]^{7-}$, such octahedral cluster would form, in any ordered pattern, four inter-cluster Ga–Ga, Ga–Li or Li–Li bonds, i.e. four-connected $[LiGa_5]^{6-}$ cluster. In such case the formula unit Ba_3LiGa_5 would be also electron balanced [14 (skeletal) +4 (two lone pairs) +4 (four inter-cluster bonds) = 22]!

In order to analyze, which of the conceptual approaches is more suitable for the description of Ba_3LiGa_5, a quantum chemical analysis of chemical bonding was applied. The following questions should be clarified: i) the presence of the lone-pairs at gallium atoms; ii) the character of the Li–Ga interactions; iii) the type of the intra-cluster bonding. In this study, the bonding analysis techniques in position space were used, which were shown recently to be a powerful bonding analysis tool, in particular for intermetallic compounds.[23–25]

The effective charges of atomic species were evaluated from the calculated electron density applying the Quantum Theory of Atoms in Molecules (QTAIM).[26] The electron density was integrated in spatial regions, which are bounded by zero-flux surfaces of the electron density gradient vector field. These electron density basins represent the atomic regions as defined in QTAIM, and their electronic populations yield the QTAIM effective atomic charges. Already the shapes of the QTAIM atoms in Ba_3LiGa_5 reveal some characteristic features (Figure 6). Usually, the barium atoms in the QTAIM representation in intermetallic compounds are represented by close to spherical shapes including mostly the inner electronic shells. As a characteristic example serve the Ba-containing clathrates.[27,28] In contrary, the shape of Ba atoms in Ba_3LiGa_5 is far from the spherical one, hinting at an appearance of unusual atomic interactions. This observation correlates with reduced QTAIM charges for barium: the observed values around +1 are considerably smaller in comparison e.g. with the charges around +1.4 in the clathrates.[27] Lithium atoms have QTAIM shapes close to spherical, the QTAIM charge of +0.74 indicates relatively high charge transfer, being similar to +0.76 in Sr_3LiAs_2H[29] and +0.83 in both modifications of SrLiAs.[30] The charge transfer found in Ba_3LiGa_5 is in agreement with all three counting schemes above. The shapes of gallium atoms reveal large almost plane faces, being characteristic for the homoatomic covalent interactions, cf. for example the QTAIM shapes of Ga in the Y–Ga compounds.[14,31]

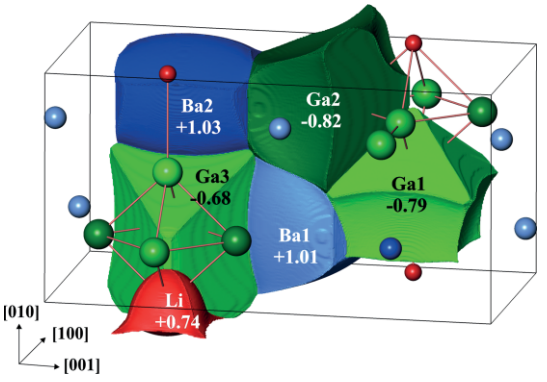

Figure 6. Shapes and effective charges of QTAIM atoms in Ba_3LiGa_5.

More insight into the atomic interactions can be obtained by the topology of ELI–D.[32] The distribution of ELI–D in the inner shells around the atomic nuclei is spherical indicating a negligible participation of these electrons in the bonding (Figure 7). The penultimate shell of barium is strongly structured, which is the second fingerprint of the considerable participation of these electrons in the bonding.[23–25] The maxima of ELI–D (attractors) in the valence region are located close to the shortest Ga–Ga and Ga–Li contacts revealing their considerable covalency. Detailed analysis involving the intersection technique[33] reveals the more complex character of these interactions. In the framework of ELI–D analysis, the procedure analogous to a QTAIM one provides electron count for each ELI–D basin. The two types of space partitioning are combined within the ELI–D/QTAIM basin intersection method to determine how ELI–D bond basins are spatially composed of QTAIM atomic regions and their electronic populations. So, the inter-cluster Ga3–Ga3 bonds are bridged by three barium atoms, which contribute 0.12 electrons to the total population of 2.12 electrons of the bonding basin. If only atoms contributing more than 10 % of the population of the bond basin are assumed to participate in the interaction, the bond may be considered as a two-atomic one. The Ga1–Li1 inter-cluster bonds are bridged by four barium atoms, and have the population of 2.64 electrons, of which 2.31 contributes Ga1 itself, 0.06 – lithium, the remaining 0.27 – the three bariums. Taking the 10 % contribution of each atom as a cut-off, this situation is considered rather as a lone pair on the gallium atom: the interpretation as a two-atomic one is not reasonable, the poly-atomic one is possible

Full Paper
doi.org/10.1002/ejic.202000413

if the cut-off above is not applied. The intra-cluster Ga2–Li1 interaction has a low bond-basin population of 0.33 electrons, the bond-basin is intersected by three atomic basins – Ga2, Li1 and Ba1 – with the contributions of 0.29, 0.02 and 0.02 electrons, respectively. Here also, the interpretation is not unambiguous: as a lone pair at Ga2 is obvious from the atomic contributions to the bond population with cut-off but the population is too low, as a three-atomic bond is possible if, cut-off is not applied, but it involves not only the cluster atoms.

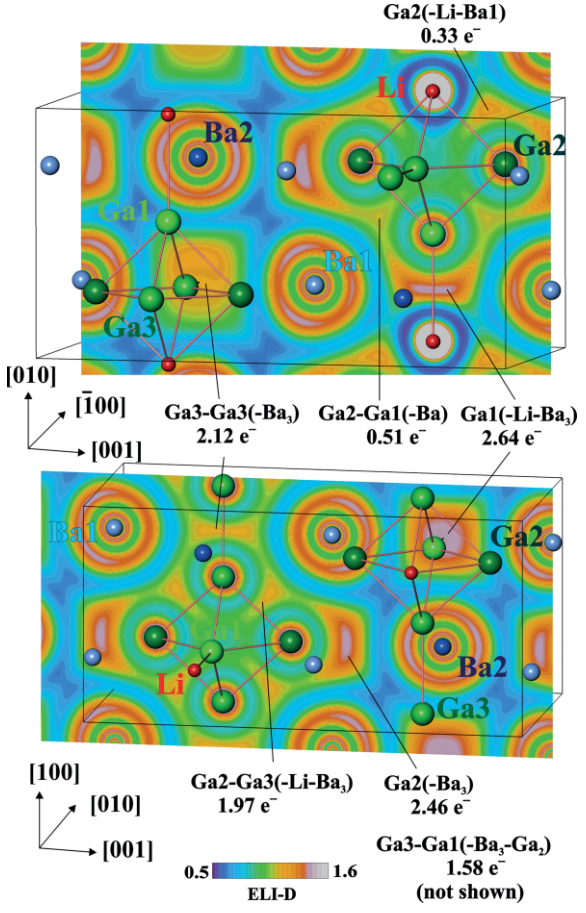

Figure 7. Electron localizability indicator in Ba_3LiGa_5: (top) distribution of ELI–D in the plane at x = 0.25; (bottom) distribution of ELI–D in the plane at y = 0.75. Atomic interactions are denoted with the atoms participating and the electronic population of the bonding basin. The atoms in parenthesis contribute less than 10 % of the basin population.

Similar situation appears also for the intra-cluster Ga1–Ga2, Ga2–Ga3 and Ga1–Ga3 interactions. The Ga1–Ga2 bond basin is intersected by the three atomic basins of (Ga1, Ga2, Ba1), but the Ba contribution is 0.01 of the 0.51 electrons in this basin. The Ga1–Ga3 basin has contributions of two Ga2 and three Ba2 atoms together are 0.17 of the total of 1.58 electrons. With cut-off, both interactions should be understood as two-atomic. The Ga2–Ga3 bond is bridged by one Li and three Ba atoms. The latter together contribute 0.12 of the total 1.97 electrons to this bond basin. The lone pair at Ga2 is surrounded by three barium atoms, they together contribute 0.30 to the basin population of 2.46 electrons: each barium delivers much less than 10 % of the population (2.5 %). There is no dedicated ELI–D attractor for the Ga3–Li1 interaction, the latter is a part of the polyatomic Ga2–Ga3 bonding (see above). The inter-cluster Ga3–Ga3 bond is bridged by three Ba atoms contributing 0.03, 0.03 and 0.05 electrons (i.e., less than 10 %) to the total population of 2.12 electrons for this bond.

In summary, the polarity of the Li–Ga interactions is very high, so that they should be understood rather as the lone pairs at the gallium atoms. The presence of the lone-pair on Ga2 atoms together with the inter-cluster Ga3–Ga3 bond clearly favors the Wade-like scheme for the understanding the chemical bonding in Ba_3LiGa_5 in comparison with the Zintl-like one. Nevertheless, in the ELI–D representation, the inter-cluster Ga–Ga bonding shows mainly two-atomic character, i.e. the Wade scheme is realized by the deficient occupation of the two-atomic bonds along the edges of the pyramidal cluster instead of the two-electron-three-atomic bonds. In this way, Ba_3LiGa_5 can be best described by means of the *nido*–[Ga_5] cluster polyanion with Ba and Li cationic counterparts. Their interaction within the gallium polyanion is multi–atomic and strongly polar.

Conclusion

The pyramidal [Ga_5] cluster in Ba_3LiGa_5 can be best understood with the Wade–Mingos rules. The compound Ba_3LiGa_5 can thus be seen as a structure with two-connected anionic *nido*–[Ga_5] clusters. Lithium plays a dual role in $BaLiGa_5$: on the one hand, it bodies for the charge compensation, and on the other one, it substitutes gallium at the same crystallographic position, thus behaving rather as a transition metal.[23] The other known precedents for this type of behavior in intermetallic compounds are the aforementioned $Eu_3Li_{5+x}Ga_{5-x}$,[5] as well as $EuLi_xGa_{2-x}$[34] and $EuLi_xGa_{4-x}$[35] where lithium substitutes gallium, forming solid solutions in binary gallides. Furthermore it has been shown that the addition of transition metals or indium instead of lithium can also lead to the formation of compounds containing octahedral gallium clusters with mixed occupied positions like $Ba_3T_xGa_{6-x}$ (T = Cu, Zn)[36] or $A_{1-2}(Ga/In)_3$ (A = K, Rb, Cs).[37]

Since the use of lithium as a component in the synthesis of ternary gallides has only been investigated marginally, Ba_3LiGa_5 can serve as starting point for a series of compounds with similar features. Additionally, a precise region for possible compositions can be found by utilizing the ΔEN vs. VEC_{Ga} diagram. This would allow for a more detailed analysis of the mixing of lithium and gallium in the identical crystallographic position, as this shows to be a common occurrence.

Experimental Section

The compound Ba_3LiGa_5 has been obtained by melting a mixture of the constituent elements barium (Alfa Aesar, 99.9 wt.%), gallium (Alfa Aesar, 99.9999 wt.%), and lithium (EVOCHEM, 99.9 wt.%). The pure metals were sealed in a tantalum crucible equipped with an intermediate sieve, which was then placed in an evacuated quartz ampule, heated to 923 K and held for 2 h for the reaction. The sample was then subsequently cooled to 723 K over 6 h and held for 120 h. Ba and Ga were used in a stoichiometric ratio and a small excess of lithium was applied to improve crystal growth and pre-

vent the formation of $BaGa_2$. The excess lithium was removed by high-temperature centrifugation-aided filtration (HTCAF) at 3000 rpm for 7 min, resulting in a single phase, polycrystalline compound. Due to the sensitivity to O_2, H_2O and N_2 the handling of the compound has been carried out completely under argon atmosphere (MBraun, O_2 < 1 ppm, H_2O < 1 ppm).

Single-crystal and powder X-ray diffraction

The structure of Ba_3LiGa_5 was solved from single-crystal X-ray diffraction data (irregularly shaped crystal glued on to a glass capillary; Rigaku AFC7 diffractometer, Saturn 724+ CCD, MoK_α radiation, λ = 0.71073 Å; multi-scan absorption correction). Additionally powder X-ray diffraction experiment was performed (25 mg of powder in a sample holder between two layers of Kapton® polyimide film with 7.5 µm thickness; Huber G670 Imaging Plate Guinier camera, Cu$K_{\alpha1}$ radiation, λ = 1.54056 Å). The unit cell parameters were refined from the X-ray powder diffraction pattern with LaB_6 as internal standard (a = 4.156916(1) Å) and subsequently used for the calculation of the interatomic distances and bonding angles. The software package WinCSD[38] was employed to perform the single crystal and individual X-ray and neutron powder diffraction solution and refinements.

Neutron powder diffraction

Elastic coherent neutron scattering experiments were performed on the high-resolution powder diffractometer SPODI at the research reactor FRM-II (Garching, Germany).[39] Monochromatic neutrons (λ = 1.5482 Å) were obtained at a 155° take-off angle using the (551) reflection of a vertically-focused composite Ge monochromator. The vertical position-sensitive multidetector (300 mm effective height) consisting of 80 ^{3}He tubes and covering an angular range of up to 160° was used for data collection. Measurements were performed in Debye–Scherrer geometry. The powder sample (ca. 5 g) was filled into a vanadium container (10 mm in diameter, 0.15 mm wall thickness) and then mounted in sample changer. The beam in front of the sample was shaped using system of slits to 40 × 20 mm vertical and horizontal cross-section. Two–dimensional powder diffraction data were collected under permanent spinning of the sample holder and then corrected for geometrical aberrations and curvature of Debye–Scherrer rings.[40] A combined refinement by using X-ray and neutron powder diffraction data (**Figure S7**) was applied to ensure the position and occupancy of the lithium atoms using the Fullprof software package.[41]

Nuclear Magnetic Resonance Spectroscopy

Nuclear magnetic resonance (NMR) experiments were performed on a Bruker Avance 500 spectrometer with a magnetic field of B_0 = 11.74 T. A standard Bruker Magic Angle Spinning (MAS) probe for 2.5 mm ZrO_2 rotors was used for the MAS and static experiments, while a custom-built probe equipped with a goniometer (NMR Service GmbH, Erfurt, Germany) was used for the pre-oriented–powder measurements. For this purpose, the crystalline sample was crushed, mixed with epoxy glue (UHU Plus Endfest 300), filled into a small quartz tube, mounted into the NMR probe and left in the NMR magnet overnight, for the glue to harden in the magnetic field. The reference frequencies for ^{7}Li and ^{71}Ga nuclei were 194.3630(0) and 152.5199(1) MHz, corresponding to the saturated solutions of LiCl and $Ga(NO_3)_3$, respectively. The spectra were obtained from the echoes after two pulses of equal duration ($90°_x - \tau - 90°_y - \tau -$ *acquisition*). The experiment–repetition times of either 30 or 60 s for ^{7}Li and between 0.25 and 1 s for ^{71}Ga were sufficient for the recovery of at least 95 % of the nuclear magnetization to the thermal equilibrium.

Thermal Analysis

Thermal analysis was performed in a glovebox under inert conditions (MBraun, O_2 < 1 ppm, H_2O < 1 ppm) with a NETZSCH STA 449 C using a DTA (/TG) HIGH RG 4/S sample holder. Ba_3LiGa_5 powder (27.47 mg) was placed in a suitable Ta crucible and covered with a lid. The sample was then heated to 973 K at a rate of 5 K min^{-1} and subsequently cooled to 473 K at the same rate.

Chemical Analysis

Three specimens of Ba_3LiGa_5 (approx. 10 mg) were weighed and dissolved in a heated mixture of 2.5 mL aqua regia and 1.1 mL H_2O_2. After the digestion process, each sample was transferred into a 50 mL volumetric flask, afterwards filled up with ultrapure water. These solutions were used for the determination of the Li amount, and in a 1:2 dilution with ultrapure water – for the amounts of Ba and Ga with the ICP-OES 5100 SVDV (Agilent), which was calibrated with matrix-matched standards. The content of oxygen and nitrogen impurities was determined with the carrier-gas-hot-extraction method. The instrument TCH600 (LECO) was calibrated with commercial steel pins as standard. The resulting values for Ba: 53.14 ± 0.37 wt.-% (calc. 53.67 wt.-%), Ga: 45.87 ± 0.29 wt.-% (calc. 45.41 wt.-%), and Li: 0.982 ± 0.004 wt.-% (calc. 0.904 wt.-%) are in good agreement with the composition obtained from the crystal structure determination. No oxygen (≤ 0.05 wt.-%) or nitrogen (≤ 0.02 wt.-%) were found within the detection limit.

Computational Methods

The electronic structure calculations were performed by using the all electron, local orbital full–potential method (FPLO) within the local density approximation.[42] The Perdew–Wang parametrization was employed.[43] The chemical disorder in Ba_3LiGa_5 is modelled using ordered unit cells set in different subgroups of the parent space group (models **1–5**). The models were optimized. All first Brillouin zones (BZ) were sampled with meshes equivalent to the mesh for model **1** (space group *Im*2*m*). The linear tetrahedron method was applied to evaluate the BZ integrals. The experimentally determined crystal structure data (Table 2) was used in the calculations.

Real-space chemical bonding analysis based on the electron localizability approach combining electron density (ED) and electron localizability indicator (ELI)[44–46] was carried out on model **2** (space group *Pnam*). The ED and Eli-D were calculated by a module implemented in the FPLO code.[47] Topological analysis of the ED and the ELI–D using the quantum theory of atoms in molecules (QTAIM)[26] was realized by the program DGrid.[32] The number of atoms contributing to a bond is determined by applying the basin intersection technique.[33]

Conflicts of interest

There are no conflicts to declare.

Acknowledgments

The authors acknowledge Dr. Frank Haarmann for the valuable discussion of the NMR results, Dr. Marcus Schmidt and Ms. Susann Scharsach for thermal analysis experiments, Dr. Gudrun Auffermann and Dipl.–Chem. Ulrike Schmidt for performing the chemical analysis, Dr. Eteri Svanidze and Dr. Primož Koželj for fruitful discussions. The funding granted to M.Kotsch by the International Max Planck Research School for Chemistry and Physics of Quantum Materials (IMPRS–CPQM) is gratefully

recognized. Open access funding enabled and organized by Projekt DEAL.

Keywords: Intermetallic phases · Clusters compounds · Zintl phases · NMR spectroscopy · Neutron diffraction

[1] C. Belin, M. Tillard-Charbonnel, *Prog. Solid State Chem.* **1993**, *22*, 59–109.
[2] B. Albert, H. Hillebrecht, *Angew. Chem. Int. Ed.* **2009**, *48*, 8640–8668; *Angew. Chem.* **2009**, *121*, 8794–8824.
[3] P. Rogl. in *Inorganic reactions and methods*, *Vol. 13* (Eds J. J. Zuckerman, A. P. Hagen), Wiley, New York, **1991**, pp. 85.
[4] T. Lundström, R. B. King, In: *Encyclopedia of Inorganic chemistry, Vol 1* (Ed.: R. A. Scott), Wiley, New York, **1994**, pp. 328–338.
[5] Fedorchuk, Yu. Prots, W. Schnelle, Yu. Grin, *Eur. J. Inorg. Chem.* **2011**, *26*, 3904–3908.
[6] Yu. Grin, A. Fedorchuk, R. J. Faria, F. R. Wagner, *Crystals* **2018**, *8*, 99.
[7] K. Schubert, F. Gauzzi, K. Frank, *Z. Metallkd.* **1963**, *54*, 422–429.
[8] D. Dayan, G. Kimmel, M. P. Dariel, *J. Nucl. Mater.* **1985**, *135*, 40–45.
[9] M. L. Fornasini, *Acta Crystallogr., Sect. C* **1983**, *39*, 943–946.
[10] Yu. Grin, R. E. Gladyshevskii, *Gallides*, Moscow, Metallurgia, **1989**.
[11] a) P. Villars, L. D. Calvert, *Pearson's Handbook of Crystallographic Data for Intermetallic Phases*, OH 44073, **1991**, 2nd edition, The Materials Information Society, Materials Park ; b) P. Villars, K. Cenzual, *Pearson's Crystal Data: Crystal Structure Database for Inorganic Compounds (on DVD)*, Release **2019**/20, ASM International®, Materials Park, Ohio, USA.
[12] CrystMet, *The Metal Database*, v. 6.0.0, **2019**, Toth Information System Inc., Ottawa.
[13] ICSD, *Inorganic Crystal Structure Database*, **2019**, v.4.2.0, Fachinformationszentrum (FIZ) Karlsruhe, Eggenstein–Leopoldshafen.
[14] R. T. Sanderson, *Inorganic Chemistry*, Reinhold Publishing Co., New York, **1967**.
[15] Yu. Grin, S. P. Yatsenko, E. G. Fedorowa, N. A. Sabirsijanow, O. M. Sitschewitsch, Y. P. Yarmolyuk, *J. Less-Common Met.* **1987**, *136*, 55–60.
[16] a) A. Iandelli, *Atti Accad. Naz. Lincei Mem. Cl. Sci. Fis. Mat. Na* **1955**, *19*, 39–43; b) F. Haarmann, K. Koch, D. Grüner, W. Schnelle, O. Pecher, R. Cardoso-Gil, H. Borrmann, H. Rosner, Yu. Grin, *Chem. Eur. J.* **2009**, *15*, 1673–1684.
[17] M. Kotsch, Yu. Prots, Yu. Grin, *XIV Conference on Crystal Chemistry of Intermetallic Compounds*, Lviv, September **2019**, Book of Abstracts, pp. 46.
[18] F. Haarmann, In: *Encyclopedia of Magnetic Resonance* (Eds.: R Laatikainen, M Tiainen, SP Korhonen, M Niemitz), John Wiley, Chichester, **2011**.
[19] P. Jeglič, M. Komelj, M. Klanjšek, U. Tkalec, S. Vrtnik, M. Feuerbacher, J. Dolinšek, *Phys. Rev. B* **2007**, *75*, 014202.
[20] C. P. Slichter, *Principles of Magnetic Resonance Vol. 3*, Springer Science & Business Media, **1989**.
[21] K. Wade, *Chem. Commun.* **1971**, *15*, 792–793.
[22] D. M. P. Mingos, *Nat. Phys. Sci.* **1972**, *236*, 99–102.
[23] F. R. Wagner, V. Bezugly, M. Kohout, Yu. Grin, *Chem. Eur. J.* **2007**, *13*, 5724–5741.
[24] Yu. Grin, In: *Comprehensive Inorganic Chemistry II*, *Vol 2* (Eds.: J Reedijk, K. Poeppelmeier), Elsevier, Oxford, **2013**, pp. 359–373.
[25] D. Bende, F. R. Wagner, Yu. Grin, *Inorg. Chem.* **2015**, *54*, 3970–3978.
[26] R. F. W. Bader, *Atoms in Molecules, A Quantum Theory*. Oxford: Clarendon Press, **1995**.
[27] H. Zhang, H. Borrmann, N. Oeschler, C. Candolfi, W. Schnelle, M. P. Schmidt, U. Burkhardt, M. Baitinger, J.-T. Zhao, Yu. Grin, *Inorg. Chem.* **2011**, *50*, 1250–1257.
[28] A. Ormeci, Yu. Grin, *J. Thermoelectr.* **2015**, *6*, 16–32.
[29] X.-J. Feng, Yu. Prots, M. Bobnar, M. P. Schmidt, W. Schnelle, J.-T. Zhao, Yu. Grin, *Chem. Eur. J.* **2015**, *21*, 14471–14477.
[30] X.-J. Feng, Yu. Prots, M. P. Schmidt, S. Hoffmann, I. Veremchuk, W. Schnelle, U. Burkhardt, J.-T. Zhao, Yu. Grin, *Inorg. Chem.* **2013**, *52*, 8971–8978.
[31] A. Fedorchuk, Yu. Grin, In: *Handbook of the Physics and Chemistry of Rare Earths*, Amsterdam, North Holland, **2018**, pp. 81–143.
[32] M. Kohout, *DGrid*, versions 4.6–5.0, **2018**.
[33] S. Raub, G. Jansen, *Theor. Chem. Acc.* **2001**, *106*, 223–232.
[34] A. Fedorchuk, Yu. Prots, W. Schnelle, Yu. Grin, *Z. Kristallogr. - Cryst. Mater.* **2005**, *220*, 315–316.
[35] A. Fedorchuk, Yu. Prots, Yu. Grin, *Z. Kristallogr. - Cryst. Mater.* **2005**, *220*, 317–318.
[36] S. Seidel, *Ph. D. Thesis*, Universität Münster, **2017**, pp. 255–264.
[37] M. Falk, C. Röhr, *Z. Kristallogr. - Cryst. Mater.* **2019**, *234*, 623–646.
[38] L. Akselrud, Yu. Grin, *J. Appl. Crystallogr.* **2014**, *47*, 803–805.
[39] M. Hoelzel, A. Senyshyn, O. Dolotko, *J. Large-Scale Research Facilities* **2015**, *1*, A5.
[40] M. Hoelzel, A. Senyshyn, N. Juenke, H. Boysen, W. Schmahl, H. Fuess, *Nucl. Instrum. Methods Phys. Res. Sect. A* **2012**, *667*, 32–37.
[41] J. Rodríguez-Carvajal, *Commission on Powder Diffraction (IUCr)* **2001**, *26*, 12–19.
[42] K. Koepernik, H. Eschrig, *Phys. Rev. B* **1999**, *59*, 1743–1757.
[43] J. P. Perdew, Y. Wang, *Phys. Rev. B* **1992**, *45*, 13244–13249.
[44] M. Kohout, *Int. J. Quantum Chem.* **2004**, *97*, 651–658.
[45] M. Kohout, *Faraday Discuss.* **2007**, *135*, 43–54.
[46] M. Kohout, F. R. Wagner, Yu. Grin, *Int. J. Quantum Chem.* **2006**, *106*, 1499–1507.
[47] Ormeci, H. Rosner, F. R. Wagner, M. Kohout, Yu. Grin, *J. Phys. Chem. A* **2006**, *135*, 1100–1105.

Received: May 17, 2020